# A FZD7-specific Antibody–Drug Conjugate Induces Ovarian Tumor Regression in Preclinical Models

Myan Do[1], Christina C.N. Wu[2], Pooja R. Sonavane[1], Edwin F. Juarez[2], Stephen R. Adams[3], Jason Ross[4], Alessandra Rodriguez y Baena[5], Charmi Patel[6], Jill P. Mesirov[2,7], Dennis A. Carson[2], Sunil J. Advani[8], and Karl Willert[1]

## ABSTRACT

Although WNT signaling is frequently dysregulated in solid tumors, drugging this pathway has been challenging due to off-tumor effects. Current clinical pan-WNT inhibitors are nonspecific and lead to adverse effects, highlighting the urgent need for more specific WNT pathway–targeting strategies. We identified elevated expression of the WNT receptor Frizzled class receptor 7 (*FZD7*) in multiple solid cancers in The Cancer Genome Atlas, particularly in the mesenchymal and proliferative subtypes of ovarian serous cystadenocarcinoma, which correlate with poorer median patient survival. Moreover, we observed increased FZD7 protein expression in ovarian tumors compared with normal ovarian tissue, indicating that FZD7 may be a tumor-specific antigen. We therefore developed a novel antibody–drug conjugate, septuximab vedotin (F7-ADC), which is composed of a chimeric human–mouse antibody to human FZD7 conjugated to the microtubule-inhibiting drug monomethyl auristatin E (MMAE). F7-ADC selectively binds human FZD7, potently kills ovarian cancer cells *in vitro*, and induces regression of ovarian tumor xenografts in murine models. To evaluate F7-ADC toxicity *in vivo*, we generated mice harboring a modified *Fzd7* gene where the resulting Fzd7 protein is reactive with the human-targeting F7-ADC. F7-ADC treatment of these mice did not induce acute toxicities, indicating a potentially favorable safety profile in patients. Overall, our data suggest that the antibody–drug conjugate approach may be a powerful strategy to combat FZD7-expressing ovarian cancers in the clinic.

## Introduction

The mammalian genome encodes 19 WNT proteins and numerous WNT receptors [including Frizzled (FZD)1–10; LRP5,6; ROR1,2; RYK, and PTK7; ref. 1), and WNT/β-catenin signaling is regulated by the intracellular β-catenin destruction complex, which includes APC (2) and AXIN (3). WNT signaling plays critical roles in embryonic development and adult tissue homeostasis by regulating stem cell renewal and differentiation (reviewed in ref. 4). Consistent with these roles, dysregulation of WNT signaling is frequently observed in human cancers. Examples of mutated or hyperactive WNT pathway components in cancer include, but are not limited to APC and AXIN; transcription factor, β-catenin (5); WNT signaling agonists, RSPO2,3 (6); and E3 ubiquitin ligase, RNF43 (7). RSPOs, RNF43, and ZNRF3, the latter also an E3 ubiquitin ligase, act by stabilizing the abundance of cell-surface receptors that mediate WNT signals. These receptors include FZD1–10, many of which have been implicated in multiple cancer histologies (reviewed in refs. 1, 8).

Pharmacologic efforts to target the WNT pathway in solid tumors have primarily focused on inhibiting WNT receptors or WNT proteins (reviewed in ref. 9). In particular, the WNT receptors FZD1, 2, 5, 7, and 8 were targeted in pancreatic, metastatic breast, and various other untreatable solid cancers by OMP-18R5 (vantictumab), a human IgG2 antibody (refs. 10–13; NIH clinical trial numbers: NCT01345201, NCT01957007, NCT01973309, and NCT02005315). Antibody–drug conjugates (ADC) have also been developed to FZD10 (OTSA101-DTPA; trial NCT04176016; ref. 14) and alternate WNT receptors, ROR1 (VLS-101, NCT03833180, NCT04504916; ref. 15), and PTK7 (PF-06647020; trial NCT03243331; ref. 16). Inhibition of pan-WNT signaling in the clinic has been achieved by two methods: using FZD8 decoy receptor, OMP-54F28 (ipafricept), to sequester extracellular WNT proteins (17–19), or by blocking Porcupine (PORCN), a protein critical to WNT secretion. Ipafricept was used in combination therapies to treat hepatocellular, liver, ovarian, and pancreatic cancers (NCT01608867, NCT02050178, NCT02069145, and NCT02092363). Many small-molecule inhibitors have been developed to inhibit PORCN, thereby inhibiting WNT secretion from cells, including WNT974/LGK974 (NCT01351103, NCT02278133, and NCT02649530), ETC-1922159 (ETC-159; NCT02521844), RXC004 (NCT03447470), and CGX1321 (NCT02675946 and NCT03507998). These PORCN inhibitors potently disrupt growth of RSPO3-translocated cancers (20), which have been observed in 10% of colon cancers (6).

Many of these WNT-targeting drugs demonstrated antitumor efficacy in patients but also induced bone-related adverse effects, likely due to the requirement for WNT signaling in bone development and homeostasis (21, 22). Trials using vantictumab (10), ipafricept (19), and ETC-159 (23, 24) were terminated due to concerns over bone-related safety or required concurrent bone-protective therapies. Such

[1]Department of Cellular and Molecular Medicine, University of California San Diego, La Jolla, California. [2]Department of Medicine, University of California San Diego, La Jolla, California. [3]Department of Pharmacology, University of California San Diego, La Jolla, California. [4]Department of Global Creative Studio, Illumina, Inc., San Diego, California. [5]Department of Biomolecular Engineering, University of California Santa Cruz, Santa Cruz, California. [6]Department of Pathology, University of California San Diego, La Jolla, California. [7]Moores Cancer Center, University of California San Diego, La Jolla, California. [8]Department of Radiation Medicine and Applied Science, University of California San Diego, La Jolla, California.

**Note:** Supplementary data for this article are available at Molecular Cancer Therapeutics Online (http://mct.aacrjournals.org/).

**Corresponding Author:** Karl Willert, University of California San Diego, 9500 Gilman Drive, MC 0695, La Jolla, CA 92093. Phone: 858-822-3235; E-mail: kwillert@health.ucsd.edu

Mol Cancer Ther 2022;21:113–24

**doi:** 10.1158/1535-7163.MCT-21-0548

bone toxicity may be side-stepped through the administration of bone-protective agents, as has been demonstrated for the PORCN inhibitor ETC-159); simultaneous treatment with alendronate, a clinically approved inhibitor of bone resorption, significantly reduced loss of bone mass (25).

An alternative strategy to alleviate bone toxicity is through more specific WNT pathway–targeting strategies. The WNT receptor Frizzled-7 (FZD7) is a strong candidate for such precise targeting due to its restricted expression pattern. FZD7 expression is largely restricted to embryonic development, with absent to modest expression in most normal adult tissues. In contrast, overexpression of FZD7 has been observed in a large number of cancer types, indicating that FZD7-specific targeting strategies may offer opportunities to treat multiple cancer types, including cancers of the stomach (26, 27), colon (28, 29), liver (30, 31), ovary (32, 33), breast (34–36), cervix (37), skin (38), and more (reviewed in refs. 39, 40).

Here, we report the development and therapeutic evaluation of a novel FZD7-targeting ADC, septuximab vedotin (F7-ADC), which consists of a chimeric human–mouse IgG1 antibody conjugated to antimitotic payload drug, monomethyl auristatin E (MMAE). We demonstrate that F7-ADC selectively and potently kills ovarian cancer cells that express high levels of FZD7 *in vitro*, as well as FZD7-high ovarian tumor xenografts *in vivo*. Importantly, we did not observe toxicities following F7-ADC treatment in mice expressing a *Fzd7* gene that has been modified to render the Fzd7 protein reactive with the human-targeting F7-ADC. Our data suggest that an ADC approach may be a powerful strategy to therapeutically attack FZD7-expressing ovarian cancers in the clinic.

## Materials and Methods

### Cell lines and culture conditions

All cell lines used in these studies were routinely tested to confirm absence of *Mycoplasma* contamination using MycoAlert Mycoplasma Detection Kit (Lonza). MA-148 (kindly provided by Prof. Sundaram Ramakrishnan, University of Miami, Miami, FL; RRID:CVCL_AK47) and MA-148 FZD7-KO were cultured in RPMI1640, 10% FBS, and 1% penicillin/streptomycin. PA-1 were obtained from ATCC (CRL-1572, RRID:CVCL_0479) and cultured in DMEM, 20% FBS, Glutamax, nonessential amino acids (NEAA), and penicillin/streptomycin. OVCAR-3 (RRID:CVCL_0465) and OVCAR-3 FZD7 were cultured in RPMI1640, 20% FBS, Glutamax, NEAA, and penicillin/streptomycin. OVCAR-3 cell line was obtained from ATCC (HTB-161). HEK293T FZD1,2,7-KO were kindly provided by Dr. Michael Boutros (Heidelberg University, Heidelberg, Germany) and cultured in DMEM, 10% FBS, and penicillin/streptomycin. Mouse embryonic fibroblasts (MEF) were cultured in DMEM, 10% FBS, Glutamax, NEAA, 25 mmol/L HEPES, and penicillin/streptomycin.

MA-148 FZD7-knock-out (KO) cells were generated by CRISPR/Cas9 knockout and screened for FZD7 expression by immunoblot and flow cytometry. MA-148 cells were transfected with pCas9-EGFP and two modified pGRNA plasmids (kindly provided by Dr. Chad Cowan, Harvard University, Boston, MA). OVCAR-3 FZD7 overexpression (OE) cells were generated by transfecting OVCAR-3 cells with pPB–EF1α:FZD7–IRES:H2B-mCherry–BlastR and pCS2-PiggyBac-Transposase.

gRNA sequence #1 for FZD7-KO: GGCCGCTCCGCTTTCGTCCC

gRNA sequence #2 for FZD7-KO: GGGCATGAGAAGGGGAAGG

### Expression vectors and cloning

7TGC (RRID:Addgene_24304); Cas9-EGFP and pGRNA (kindly provided by Dr. Chad Cowan, Harvard University, Boston, MA; pcDNA3.4-TOPO FZD7 IgG1 antibody (F7-Ab) heavy chain; pcDNA3.4-TOPO F7-Ab light chain; pCS2-PiggyBac-Transposase; pLVX-Luciferase-PuroR (kindly provided by Drs. Ian Huggins and Steve Dowdy, UC San Diego, San Diego, CA); pPB–EF1α:FZD7–IRES:H2B-mCherry–BlastR.

### ADC synthesis

F7-Ab-MMAE drug conjugate was synthesized using methods previously described (41, 42). A solution (2 mL, 10.2 mg/mL) of F7-Ab was treated with sodium bicine buffer (200 μL, 1 mol/L pH 8.3) and sodium diethylenetriaminepentaacetic acid (20 μL, 100 mmol/L pH 7) following reduction with 4 equivalents of tris(carboxyethyl) phosphine (TCEP) at 37°C for 2 hours, the solution was added to four equivalents of maleimidocaproyl-valine-citrulline-PABC-MMAE (MC-VC-PABC-MMAE, Levena Biopharma). After 30 minutes at room temperature, Cy5-maleimide (2 equivalents) was added and after a further 30 minutes, gel-filtered (Sephadex G25, 1.0 g) eluting with phosphate buffered saline (PBS). Following centrifugal concentration (Centricon 30 kDa MWCO) to about 500 μL, the concentrations of antibody and Cy5 were determined by absorbance using extinction coefficients of 251,000 $M^{-1}$ $cm^{-1}$ (F7-Ab) at 280 nm and 12,500 $M^{-1}$ $cm^{-1}$ and 250,000 $M^{-1}$ $cm^{-1}$ at 280 nm and 650 nm respectively, for Cy5. Drug loading was measured by denaturing reverse-phase HPLC of the reaction mix prior to addition of Cy5 maleimide, following reduction of any remaining intersubunit disulfides with 50 mmol/L DTT for 30 minutes. Peaks corresponding to light or heavy chains with 0–3 MMAE were identified by electro-spray mass spectroscopy and peak areas at 280 nm were integrated and weighted to calculate the drug loading. Modified light chain (L1) and unmodified H chain (H0) were not resolved so MMAE loading is an underestimate. No free MC-VC-PABC-MMAE was detected by HPLC following gel filtration.

### Flow cytometry

Cells were dissociated using Accutase (Innovative Cell Technologies, RRID:AB_2869384), pelleted, resuspended in FACS buffer (PBS, 5 mmol/L EDTA, and 2% FBS), and passed through a 40-μm cell strainer (Corning). $1\times10^5$ cells were incubated on ice for 30 minutes with the indicated concentrations of F7-ADC or F7-Ab-Alexa Fluor 647. Cells were washed with 3 mL of FACS buffer, pelleted, and resuspended in FACS buffer with 0.5 μg/mL DAPI (Cell Signaling Technology). Cells were analyzed on an LSRFortessa (BD Biosciences) and FSC files were processed using FlowJo (BD Biosciences).

### qRT-PCR

qRT-PCR methods and primer sequences (*FZD7*, *RPL13A*) were used as previously described (43).

### Confocal live imaging

Imaging of ADC internalization was performed as previously described (41). In brief, cells were seeded on a glass-bottom plate for imaging. Cells were washed with PBS, then treated with a vehicle control (PBS) or F7-ADC in 1% FBS media at 37°C for 3 hours. Cells were washed with PBS and replenished with regular 10% FBS media and 50 nmol/L Lysotracker Green (Invitrogen). Live imaging was performed for 1 hour after media replenishment on a Nikon Eclipse Ti2-E or Nikon CSU-W1 microscope with a Plan Apo Lambda 60 ×1.4NA objective.

### Cytotoxicity assay

Cells were seeded in a 96-well plate the day before drug treatment. MA-148, PA-1, and MA-148 FZD7-KO were incubated with the indicated drugs for 3 days. OVCAR-3 and OVCAR-3 FZD7 were incubated for 5 days due to slower doubling time compared with the other three cell lines. Drug-containing media were then removed, replaced with 100 μL RPMI1640 and 100 μL of CellTiter-Glo2.0 per well, and incubated in the dark for 25 minutes. CellTiter-Glo2.0 luciferase readouts were performed on a Promega GloMax Discover Microplate Reader.

### *Fzd7*$^{hF7/hF7}$ mouse line generation

*Fzd7*$^{hF7/hF7}$ mice were generated by standard CRISPR/Cas9 methods by Transgenic Mouse Services at UC San Diego (UCSD, San Diego, CA) and in compliance with UCSD Institutional Animal Use and Care Committee (IACUC). C57BL/6NHsd mouse embryos were injected with a Fzd7 repair oligo, Fzd7 guide RNA (gRNA), and Cas9 mRNA (Invitrogen). The repair oligo was synthesized by Integrated DNA Technologies. The *in vitro* transcribed gRNA was generated using a MEGAscript T7 Transcription Kit (Thermo Fisher).

Fzd7 repair oligo (underlined: new *Bgl*II site; bolded: changed nucleotides):

GACGGCTCCGGGGGCGCGGGCGGCAGTCCCACCGCCT-ACCCTACTGCTCCCTACCTGCCAGA**TCT**ACCTTTCA-CTGCGATGTCCCCCTCAGATGGCAGAGGCCGCTTGT-CTTTCCCCTTCTCGTGTCCGCGC

Fzd7 guide RNA (Underlined: PAM sequence): GGGGACATCG-CAGTGAAAGG(TGG)

### MEF generation

All animal studies have been conducted in accordance with, and with the approval of, an IACUC (protocol number S05387, PI: K. Willert). MEFs were generated from decapitated E13.5 embryos. 7–8 embryos per genotype were minced in warm trypsin for 10 minutes, washed with trypsin, and pipetted up and down. DNase (Promega) was added to the embryo suspension, pipetted up and down three times, and incubated at 37°C for 5 minutes. MEF medium was added to the suspension, pipetted up and down, and centrifuged at 1,000 × *g*. Supernatant was removed and the dissociated embryo pellet was resuspended in MEF medium and plated for cell expansion.

### Immunoblot

Immunoblot methods and antibody dilutions were used as previously described (43).

### Wnt reporter (TOP-GFP) assay

Primary MEFs at passage 3 (P3) were transduced with third-generation lentivirus containing 7TGC (Addgene 24304) and then passaged. P4 MEFs were treated with Wnt3a storage buffer (PBS, 1% CHAPS, 1 mol/L NaCl), 5 nmol/L Wnt3a, or 5 nmol/L F7L6. Cells were dissociated using Accutase, pelleted, resuspended in FACS buffer with 0.5 μg/mL DAPI (Cell Signaling Technology), and passed through a 40-μm cell strainer (Corning). Cells were analyzed on an LSRFortessa (BD Biosciences) and FSC files were processed using FlowJo (BD Biosciences).

### *In vivo* tumor xenograft response studies

All animal studies have been conducted in accordance with, and with the approval of, an IACUC (protocol number S05387, PI: K. Willert). Six-week-old female nude mice were purchased from the UC San Diego Animal Care Program breeding colony. MA-148-Luciferase (Luc), PA-1-Luciferase, or MA-148 FZD7-KO-Luciferase cells were injected in the bilateral upper thigh to establish subcutaneous tumors. For MA-148-Luciferase or MA-148 FZD7-KO-Luciferase tumors, $3 \times 10^6$ cells were suspended in 100 μL of a 1:1 mix of Matrigel and 10% FBS media. For PA-1-Luciferase tumors, $5 \times 10^6$ cells were suspended in 100 μL of a 1:1 mix of Matrigel (BD Biosciences) and 10% FBS media. Tumor bioluminescence was measured by an IVIS Spectrum (Perkin Elmer) after intraperitoneal injection of XenoLight D-luciferin (Perkin Elmer; 200 μL of a 15 mg/mL stock). Tumor bioluminescence was normalized to background bioluminescence of a non–tumor-bearing mouse injected with luciferin. Mice were randomized into groups once normalized tumor bioluminescence (radiance) reached at least $1 \times 10^7$ photons/second. In Vivo Imaging System (IVIS) analyses were performed using Living Image software (Perkin Elmer). Treatments were delivered twice per week by bilateral tail vein injection. To prevent unnecessary morbidity, mice were euthanized if tumor length exceeded 15 mm by caliper measurement.

### *In vivo* toxicity study

All animal studies have been conducted in accordance with, and with the approval of, an IACUC (protocol number S05387, PI: K. Willert). Twelve-week-old *Fzd7*$^{hF7/hF7}$ and *Fzd7*$^{+/+}$ mice were treated with F7-ADC (10 mg/kg) by bilateral tail vein injection. Seven days after injection, mice were euthanized and tissues collected. All tissues were fixed in 4% paraformaldehyde (PFA) for 24 hours at 4°C. Brains were transferred to a 30% sucrose solution and all other tissues were transferred to 70% ethanol (EtOH) and stored at 4°C. Blood samples were analyzed by ELISA as described below.

### Hematoxylin and eosin staining

Hematoxylin and eosin (H&E) staining was done by UCSD Tissue Technology Shared Resource (TTSR) on a Thermo Gemini AS Stainer. Tissues were baked at 60°C for 1 hours and transferred to solutions in the following order: Clearite-3 (Thermo Fisher), 100% EtOH, 95% EtOH, di$H_2O$, hematoxylin (Thermo Fisher), di$H_2O$, Clarifier 1 (Thermo Fisher), di$H_2O$, Bluing Solution (Thermo Fisher), di$H_2O$, 70% EtOH, Eosin-Y (Thermo Fisher), 70% EtOH, 95% EtOH, 100% EtOH, Clearite-3, mounting medium (VWR).

### IHC

OV801a ovarian cancer tissue array with matched or unmatched adjacent normal tissue was purchased from US Biomax. IHC was done by UCSD TTSR. Tumor samples were fixed in 4% PFA at 4°C, and transferred to 70% EtOH. Tissues were baked at 60°C for 1 hour, then cleared and rehydrated through successive solutions: xylene, 100% EtOH, 95% EtOH, 70% EtOH, di$H_2O$. Antigen retrieval was performed in Antigen Unmasking Solution (Vector) at 95°C for 30 minutes. Staining was performed on Intellipath Automated IHC Stainer (Biocare): tissues were blocked in Peroxidase Bloxall (Vector), washed in Tris buffered saline with 0.2% Tween-20 (TBST), and blocked in 3% donkey serum for 10 minutes. Primary antibody incubations were for 1 hour with F7-Ab (2.5 μg/mL) for cancer tissue array, and rabbit anti-Ki67 (GeneTex, catalog no. 16667, 1:50, RRID: AB_422351) for tumor samples. Tissues were then processed as follows: TBST washes, anti-mouse EnVision+ System-HRP Labeled Polymer (Dako) or anti-rabbit HRP Polymer (Cell IDx) for 10 minutes, TBST washes, DAB Chromogen (VWR) for 5 minutes, di$H_2O$ washes,

Mayer Hematoxylin (Sigma) for 5 minutes, TBST washes, di$H_2O$ washes, cleared, and mounted in xylene-based mounting media.

### ELISA

Detection of human IgG in mouse serum samples was performed using the IgG (Total) Human Uncoated ELISA Kit (Invitrogen) according to manufacturer's protocol.

### Statistical analyses

Details on statistical tests used for each experiment are provided in corresponding figure legends.

### The Cancer Genome Atlas analyses

RNA-sequencing (RNA-seq) counts [transcripts per million (TPM) normalized] were obtained from ref. 44. The median TPM value of each gene in each cancer type was computed and $\log_2$-normalized values are plotted. For the ovarian serous cystadenocarcinoma (OV) dataset, classification of samples was obtained from (45). The BRCA dataset was classified by the reported histopathology status of each patient. For a reproducible version of the code used for these analyses, visit:

https://notebook.genepattern.org/services/sharing/notebooks/409/preview/
https://notebook.genepattern.org/services/sharing/notebooks/410/preview/
https://notebook.genepattern.org/services/sharing/notebooks/411/preview/
https://notebook.genepattern.org/services/sharing/notebooks/412/preview/

### Data availability

The data generated in this study are available within the article and its Supplementary Data files.

## Results

### FZD7 RNA and protein expression are elevated in ovarian carcinomas

To evaluate expression of *FZD7* across human cancers, we interrogated bulk RNA-seq patient datasets in The Cancer Genome Atlas (TCGA; **Fig. 1A**). We found elevated median *FZD7* expression in breast invasive carcinoma (BRCA), glioblastoma multiforme (GBM), lung squamous cell carcinoma (LUSC), ovarian serous cystadenocarcinoma (OV), prostate adenocarcinoma (PRAD), and uterine carcinosarcoma (UCS) studies. We then further analyzed TCGA OV and BRCA datasets. We separated OV samples into four subtypes defined by "Classification of Ovarian Cancer" (CLOVAR), a prognostic model for high-grade serous ovarian carcinoma (45). Median *FZD7* expression was higher in the mesenchymal and proliferative subtypes (**Fig. 1B**), which correlated with a median survival of ∼36 months in patients (45). In contrast, median survival for the differentiated and immunoreactive subtypes was approximately 48 months (45). We also separated BRCA samples based on reported histopathology status and identified higher *FZD7* expression in triple-negative breast cancer (Supplementary Fig. S1), which also has been associated with poor prognosis (that is, decreased disease-free survival and overall survival; ref. 46). In addition, we analyzed FZD7 protein expression by IHC and observed higher levels in ovarian carcinomas compared with normal ovarian tissues (**Fig. 1C**), indicating that FZD7 may represent a tumor-specific antigen. By mining TCGA data and performing histologic analyses, we confirmed that FZD7 is a viable candidate for targeted cancer therapies against the WNT pathway and importantly for clinically aggressive subtypes of ovarian and breast cancer.

### ADC septuximab vedotin binds FZD7

To target human FZD7, we developed an ADC, septuximab vedotin, hereafter referred to as F7-ADC. We previously demonstrated that the chimeric human–mouse IgG1 antibody to FZD7 (F7-Ab) binds FZD7 and does not cross-react with the other nine human FZD receptors, FZD(1–6,8–10) (43, 47). F7-ADC consists of F7-Ab conjugated to the antimitotic drug MMAE, by cleavable MC-VC-PABC linkers (**Fig. 2A**). An average of four MMAE molecules were conjugated to cysteine residues in the antibody hinge region, following reduction of disulfides (41, 42). For noninvasive F7-ADC tracking, we also conjugated a Cy5 fluorophore to a hinge region disulfide via a noncleavable maleimide linker. MMAE drug loading was measured by denaturing reverse-phase HPLC and electro-spray mass spectroscopy (Supplementary Fig. S2). By flow cytometry, we confirmed that F7-ADC bound to FZD7-high (MA-148, PA-1, and OVCAR-3 FZD7) and FZD7-low (OVCAR-3) human cancer cell lines, but did not bind MA-148 FZD7-knockout (KO) cells (**Fig. 2B** and **C**). FZD7 RNA levels in these cell lines directly correlated with protein levels (**Fig. 2D**). These data demonstrate that F7-ADC specifically bound human cancer cells expressing FZD7.

### Septuximab vedotin selectively targets and kills FZD7-expressing cells *in vitro*

ADCs constructed with MC-VC-PABC linkers function by binding cell membrane receptors which are then internalized into lysosomes of target-expressing cells. Within lysosomes, cathepsin B cleaves the valine-citrulline dipeptide of the MC-VC-PABC linker followed by PABC self-immolation and release of the drug (48). To confirm that F7-ADC internalized to the lysosomes of FZD7-expressing cancer cells, we treated FZD7-positive and FZD7-negative cells with a vehicle control (PBS) or F7-ADC and performed confocal live imaging. We observed colocalization of F7-ADC and lysosomes specifically in FZD7-positive MA-148, PA-1, and OVCAR-3 FZD7 cells, but not in the MA-148 FZD7-KO cells (**Fig. 3A**).

Next, we tested F7-ADC–specific cytotoxicity *in vitro* (**Fig. 3B**). A single dose of F7-ADC killed MA-148 and PA-1 cells at an $IC_{50}$ of 5 nmol/L (0.76 μg/mL), and OVCAR-3 FZD7 cells at an $IC_{50}$ of 0.025 nmol/L (3.9 ng/mL). The $IC_{50}$ for OVCAR-3 and MA-148 FZD7-KO cells were 25 nmol/L (3.9 μg/mL) and 60 nmol/L (9.6 μg/mL), respectively. At concentrations tested, treatment with unconjugated F7-Ab did not affect the viability of cells, suggesting that the naked F7-Ab does not interfere with FZD7 functions critical to cell survival. These results established a therapeutic window in which F7-ADC specifically internalized and killed FZD7-expressing cells *in vitro*.

### Septuximab vedotin induces regression of FZD7 tumors *in vivo*

To test *in vivo* efficacy of the human-targeting F7-ADC, we utilized xenograft tumor models. We established MA-148, PA-1, or MA-148 FZD7-KO subcutaneous tumors expressing a luciferase reporter, in athymic nude mice. Tumor volume was measured by bioluminescence detection using an IVIS. Mice were treated twice per week with a vehicle control or F7-ADC (3 mg/kg; ∼0.5 nmol/L) by intravenous (tail vein) injection. In MA-148-Luciferase and PA-1-Luciferase tumors, F7-ADC treatment resulted in significant tumor regression (**Fig. 4A**, **B** and **D**). In contrast, F7-ADC had no therapeutic effect on MA-148 FZD7-KO-Luciferase tumor growth because they continued

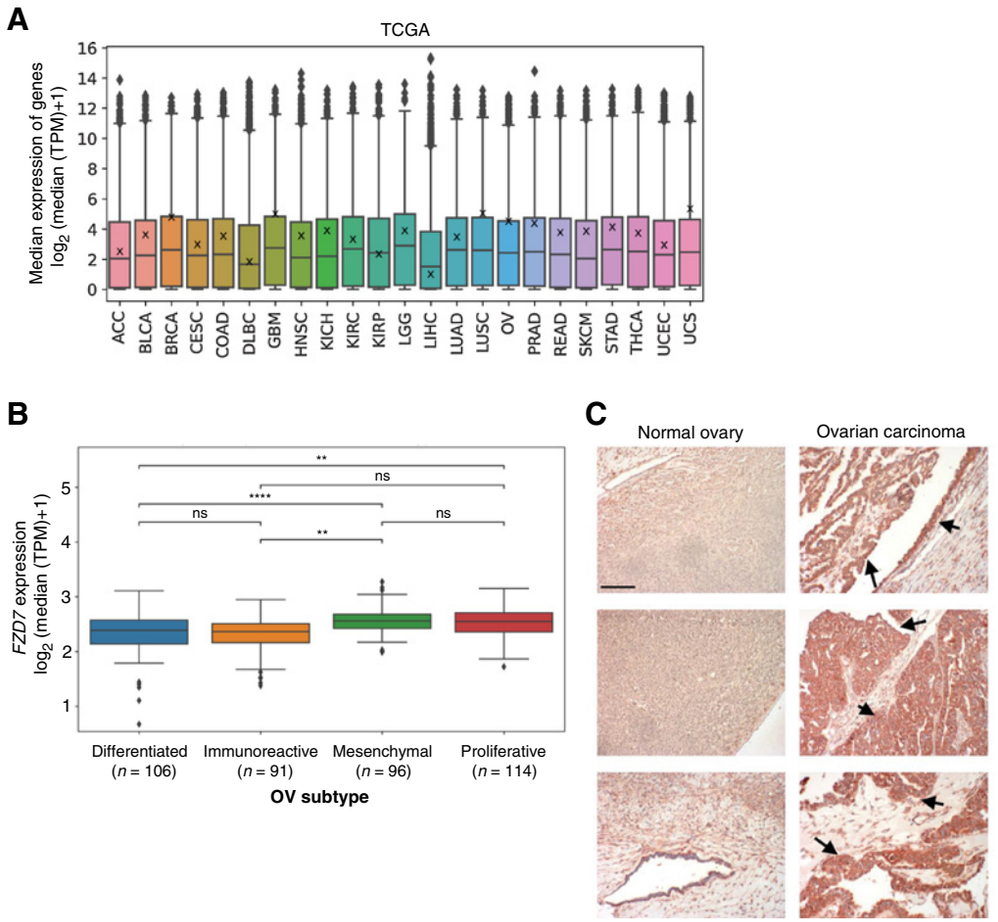


**Figure 1.**

*FZD7* RNA and protein expression are elevated in ovarian carcinomas. **A,** Median *FZD7* expression in TCGA RNA-seq by cancer type. Data points indicate individual genes; box plots indicate 75% of surveyed genes; X's on box plots indicate *FZD7* expression. **B,** Median *FZD7* expression in TCGA OV subtypes defined by CLOVAR. Data points indicate individual patient samples; box plots indicate 75% of surveyed patient samples. For statistical analyses: two-sided Mann–Whitney–Wilcoxon test with Bonferroni correction; ****, $P \leq 0.0001$; **, $P \leq 0.01$; ns, not significant. **C,** FZD7 expression is low in normal ovarian tissues but elevated in ovarian carcinomas. Tissues shown at 100× magnification; red-brown staining and arrows: FZD7 staining; scale bar, 500 μm.

to grow exponentially (**Fig. 4C**), similarly to the vehicle-treated tumors. IHC at the conclusion of the study showed a marked reduction in staining of the proliferation marker Ki67 in MA-148 and PA-1 tumors, but not in MA-148 FZD7-KO tumors (Supplementary Fig. S3).

## Generation of *Fzd7$^{hf7/hF7}$* mice

We previously identified the extracellular epitope on human FZD7 to which our antibody (F7-Ab) binds (43), mapping to the linker region between the ligand binding cysteine rich domain and the first transmembrane domain of FZD7. Moreover, we found that a single amino acid change (proline to leucine at position 188, P188L) in mouse Fzd7 rendered Fzd7 reactive with F7-Ab. We used CRISPR-Cas9 to engineer the P188L mutation in mouse *Fzd7* (**Fig. 5A** and **B**). The resulting mouse line, *Fzd7$^{hF7/hF7}$*, expresses Fzd7$^{P188L}$ receptors that are recognized by F7-Ab (**Fig. 5C**). *Fzd7$^{hF7/hF7}$* mice are viable, fertile, and do not exhibit any of the phenotypic abnormalities previously described in *Fzd7* knockout mice, including tail truncation and kinking (49), suggesting that the *Fzd7$^{hF7/hF7}$* allele produces a functional Fzd7$^{P188L}$ protein.

To establish that Fzd7$^{P188L}$ is functional, we tested its ability to transduce Wnt signaling *in vitro*. We derived MEFs from E13.5 *Fzd7$^{+/+}$* (wild type) and *Fzd7$^{hF7/hF7}$* embryos and transduced them with Wnt reporter, 7TGC (TOP-GFP:SV40-mCherry; ref. 50). To selectively activate Fzd7$^{P188L}$, we used a previously described WNT mimetic, F7L6 (43), which only interacts with human FZD7. MEFs carrying the 7TGC reporter were treated with a Wnt buffer control, F7L6, or Wnt3a. We quantified reporter GFP activity from mCherry-expressing MEFs using flow cytometry and confirmed that *Fzd7$^{hF7/hF7}$* MEFs responded to F7L6 and Wnt3a. In contrast, Wnt reporter activity in *Fzd7$^{+/+}$* MEFs was only stimulated by Wnt3a and not F7L6 (**Fig. 5D**). These results indicate that *Fzd7$^{hF7/hF7}$* mouse line expressing Fzd7$^{P188L}$ receptors retain Wnt signaling capability.

## Septuximab vedotin does not induce toxicity in *Fzd7$^{hf7/hF7}$* mice

To evaluate for potential toxicities induced by human-FZD7-targeting F7-ADC, we tested F7-ADC in *Fzd7$^{hF7/hF7}$* mice. On day 0, we gave a single tail vein injection of F7-ADC (10 mg/kg) in 12-week-old females and males of *Fzd7$^{hF7/hF7}$* and *Fzd7$^{+/+}$* genotype. Uninjected control mice for each sex and genotype were also

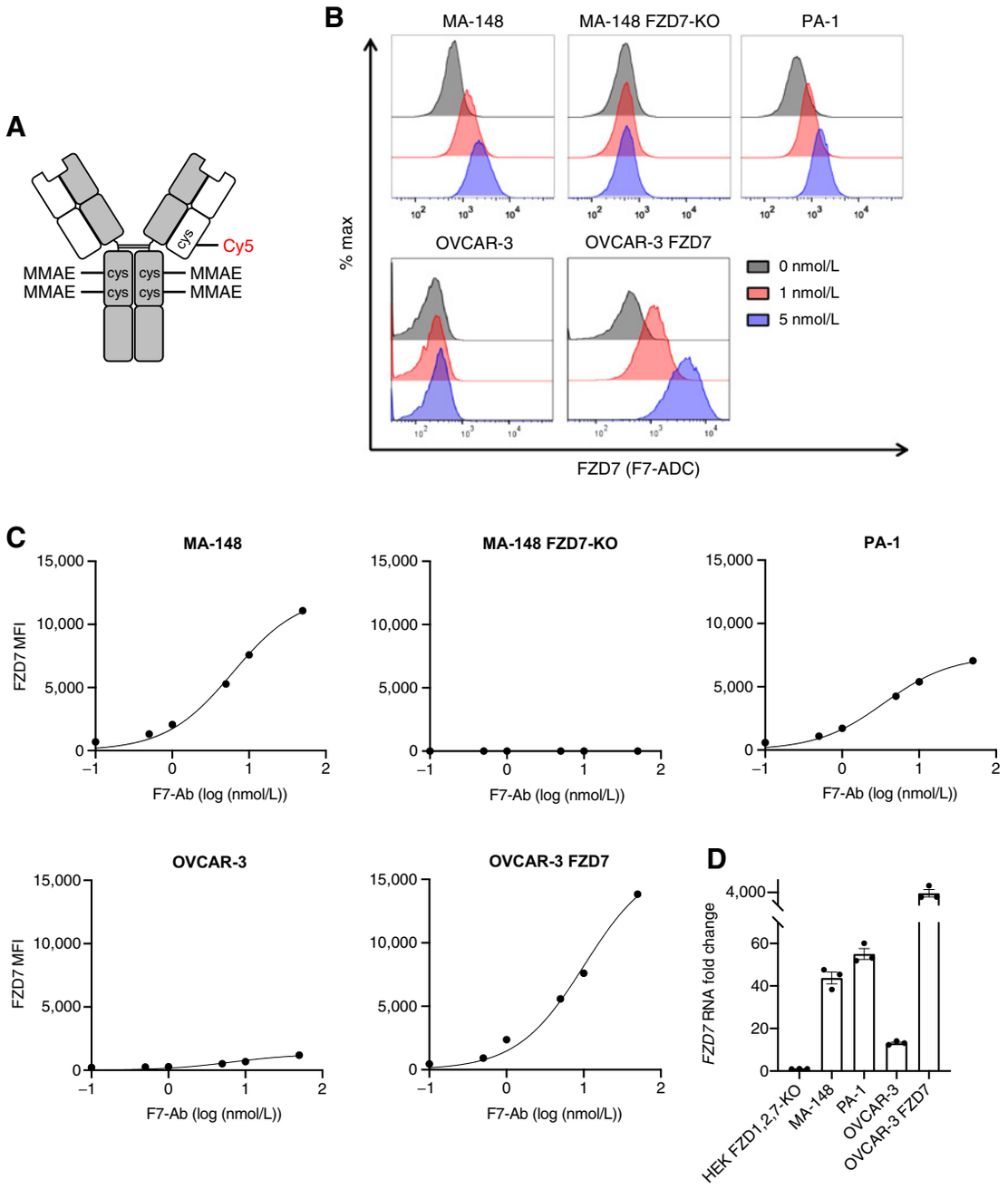


**Figure 2.**

ADC septuximab vedotin binds FZD7. **A,** Schematic of ADC, septuximab vedotin (F7-ADC). MC-VC-PABC-MMAE and Cy5 are conjugated to the IgG1 antibody at cysteine (cys) residues. **B,** F7-ADC selectively binds FZD7-expressing human cancer cell lines, MA-148, PA-1, OVCAR-3, and OVCAR-3 FZD7. F7-ADC does not bind MA-148 FZD7-KO. Live cells were stained with F7-ADC at the indicated concentrations and analyzed by flow cytometry. **C,** FZD7 protein expression represented as mean fluorescence intensity (MFI). Live cells were stained with F7-Ab and analyzed by flow cytometry. **D,** *FZD7* expression by qRT-PCR and normalized to HEK293T (HEK) FZD1,2,7-KO. Data represented as mean ± SEM for three technical replicates.

included (**Table 1**). $Fzd7^{+/+}$ mice were used as additional negative controls since F7-ADC does not recognize wild-type mouse Fzd7. Neither F7-ADC–treated $Fzd7^{hF7/hF7}$ or $Fzd7^{+/+}$ mice exhibited changes in activity levels or grooming behavior 2 hours postinjection and over the following 7 days, compared with uninjected control mice (**Table 1**; Supplementary Fig. S4). In addition, we did not observe diarrhea or concerning changes in weight between days 0 and 7. To determine whether the high dose of F7-ADC induced damage at the tissue level, we euthanized the mice on day 7 postinjection at which time brain, eye, heart, kidney, liver, ovary or

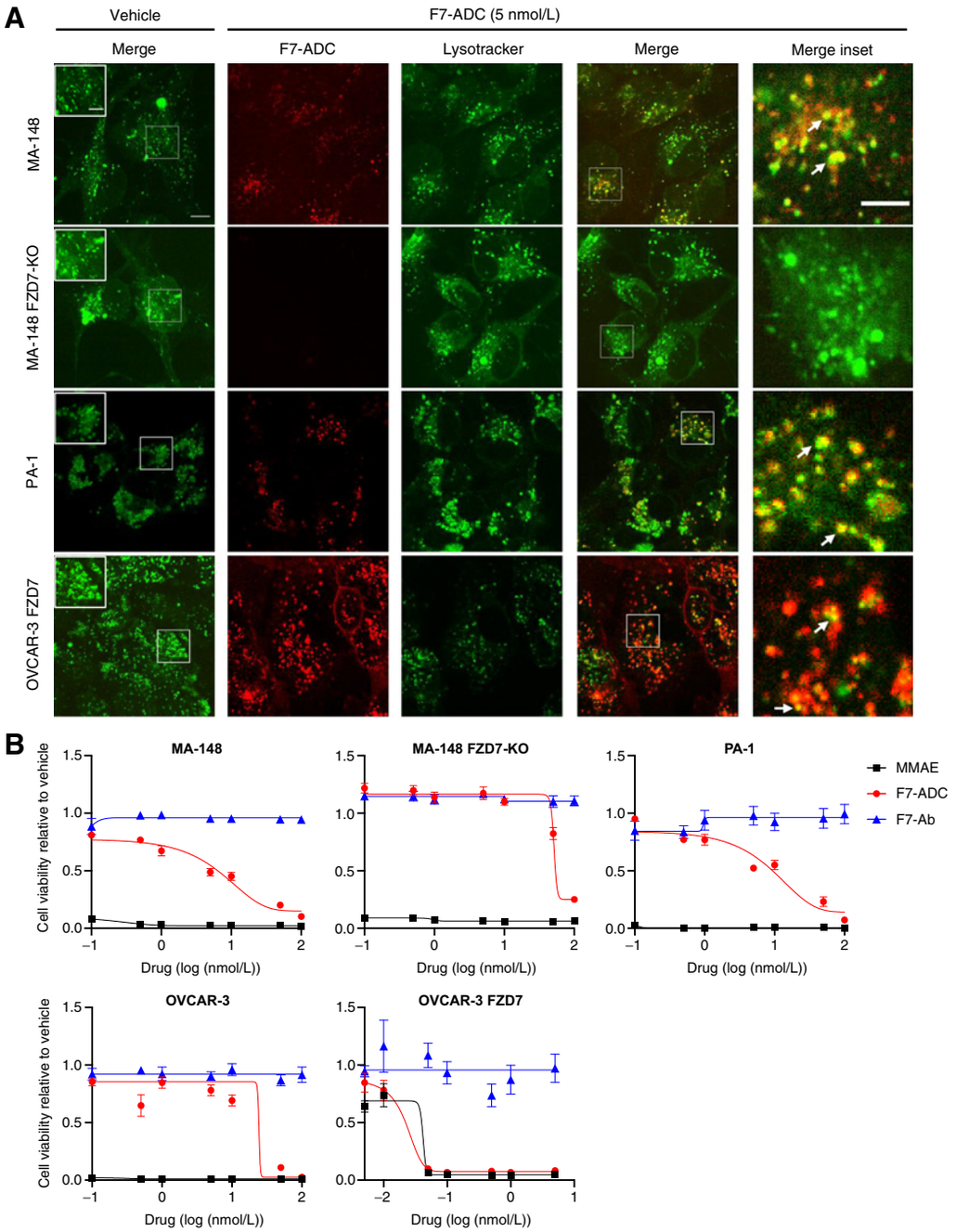


**Figure 3.**

Septuximab vedotin specifically targets and kills FZD7-expressing cells *in vitro*. **A,** Colocalization of F7-ADC and lysosomes was observed after 1 hour in FZD7-positive MA-148, PA-1, and OVCAR-3 FZD7, but not in MA-148 FZD7-KO. Arrows, colocalization; scale bar, 10 μm; inset scale bars, 5 μm. **B,** F7-ADC induced direct, FZD7-dependent cytotoxicity in a cell viability assay. Cells were treated with 0.1–100 nmol/L (0.0016–16.4 μg/mL) of indicated drug and all viability were normalized to vehicle. Data represented as mean ± SEM for two independent experiments, three technical replicates per experiment.

testis, skin, small intestine, and spleen were harvested. Sections of the organs from $Fzd7^{hF7/hF7}$ and $Fzd7^{+/+}$ mice were H&E stained and reviewed digitally from 2× to 40× magnification. No histopathologic abnormalities were noted in any organs, specifically no areas of necrosis, fibrosis, calcification, increased inflammatory infiltrates, edema, dysplastic changes or carcinoma were detected (representative images of the intestine, ovary, skin, and liver in Supplementary Fig. S4). Importantly, we did not observe damage to the crypt or villi structures within the small intestine, where Fzd7 is expressed in $Lgr5^{+}$ stem cells (51, 52). Furthermore, presence of human IgG in serum from all mice at the time of euthanasia was confirmed using quantitative ELISAs (Supplementary Fig. S5).

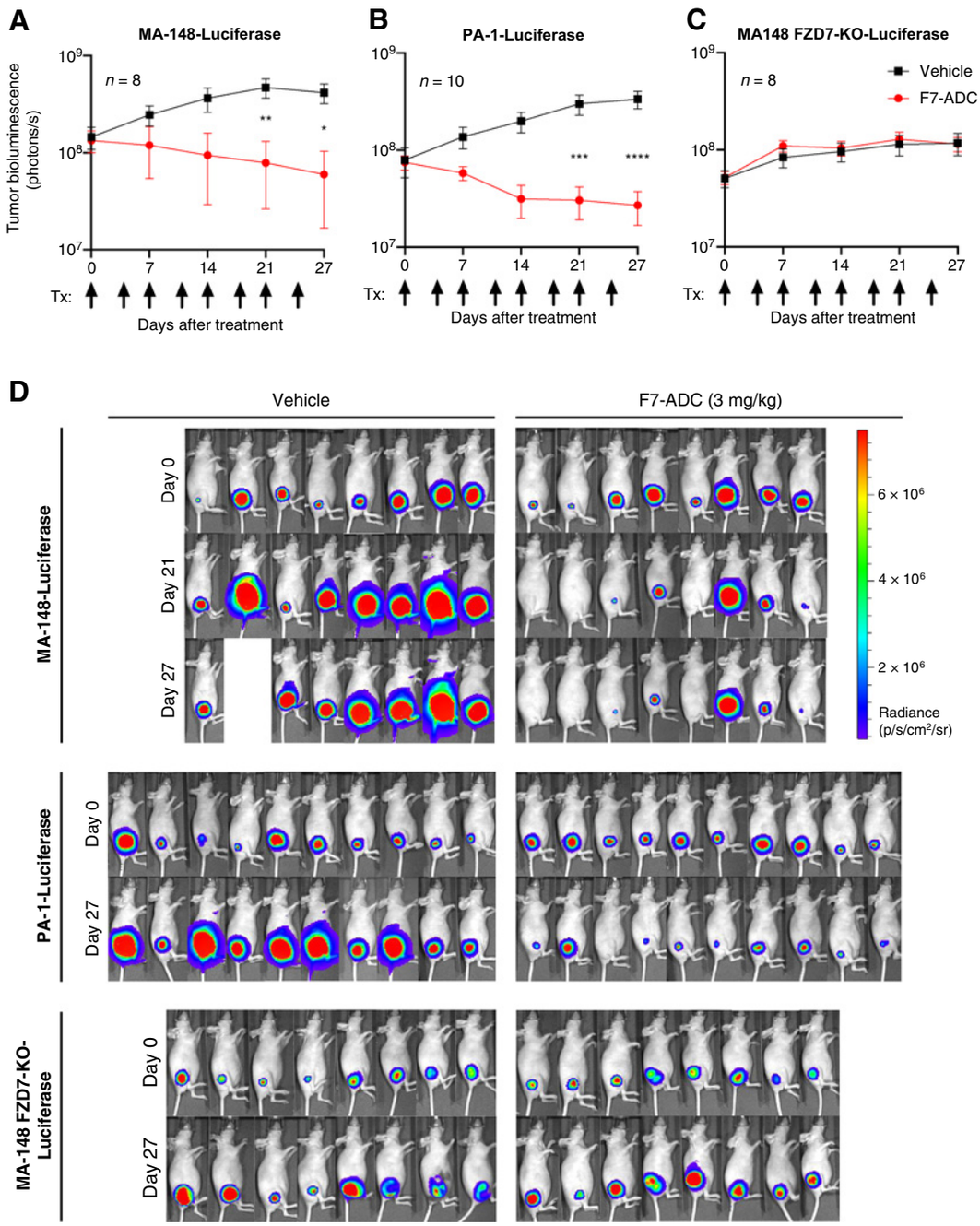


**Figure 4.**

Septuximab vedotin induces regression of FZD7 tumors *in vivo*. **A,** MA-148-Luciferase and **B,** PA-1-Luciferase subcutaneous tumor xenografts treated with F7-ADC (3 mg/kg; ∼0.5 nmol/L) regressed after 6 doses of ADC (one vehicle MA-148-Luciferase mouse was euthanized prior to day 27 due to the tumor diameter exceeding 15 mm). **C,** F7-ADC-treated MA-148 FZD7-KO-Luciferase tumors were not statistically different from vehicle-treated tumors. Tumor IVIS data represented as mean ± SEM; arrows indicate days of treatment (Tx). For statistical analyses: one-way ANOVA and Tukey multiple comparisons test: ****, $P \le 0.0001$; ***, $P \le 0.001$; **, $P \le 0.01$; *, $P \le 0.05$. **D,** IVIS images for each tumor type.

## Discussion

Although aberrant WNT signaling is observed in many solid tumor histologies, pharmacologically drugging the WNT pathway for therapeutic gain has proved to be a clinical challenge. Most WNT-targeting therapies aimed to globally inhibit WNT signaling, frequently resulting in bone-related adverse effects in patients. In an effort to mitigate toxicities associated with WNT inhibition, we developed an ADC, septuximab vedotin (F7-ADC), to target and kill human cancer cells expressing WNT receptor, FZD7. In bulk RNA-seq analyses of TCGA

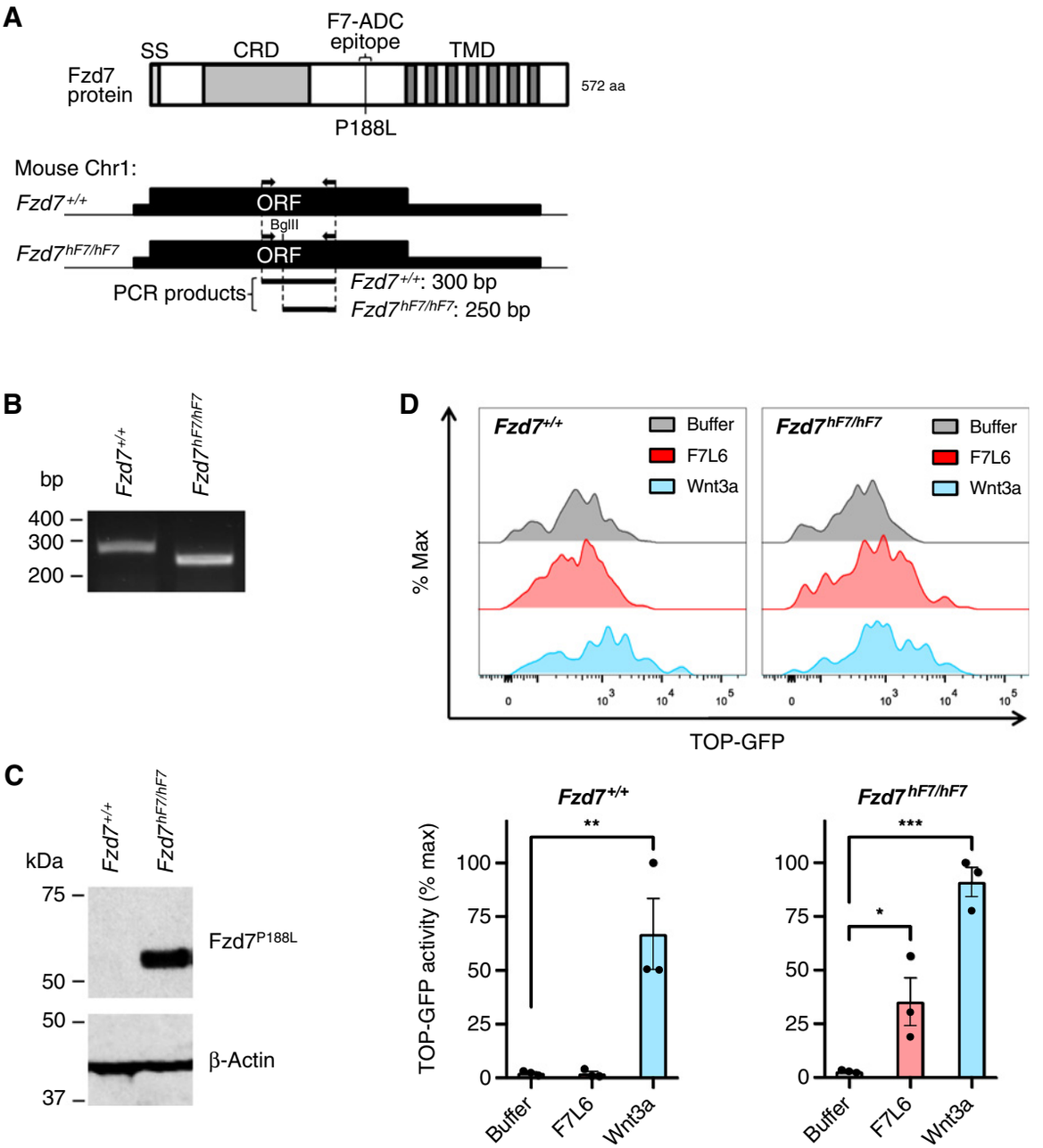


**Figure 5.**

Generation of *Fzd7*$^{hF7/hF7}$ mice. **A,** Schematic of genotyping strategy for *Fzd7*$^{hF7/hF7}$ mice. Top, domain structure of mouse Fzd7 protein. Bottom, genomic region of *Fzd7* gene on mouse chromosome 1. Arrows indicate position of PCR primers for genotyping. Restriction enzyme BglII digests the PCR product generated from the *Fzd7*$^{hF7/hF7}$ allele only. Abbreviations: aa, amino acids; bp, base pairs; CRD, cysteine rich domain; *Fzd7*$^{+/+}$, wild type; ORF, open reading frame; SS, signal sequence; TMD, transmembrane domain. **B,** Genotyping of *Fzd7*$^{+/+}$ and *Fzd7*$^{hF7/hF7}$ alleles. PCR and *Bgl*II digest of genomic DNA produces a 300-bp fragment for *Fzd7*$^{+/+}$ and 250-bp fragment for *Fzd7*$^{hF7/hF7}$. **C,** Immunoblot of cell lysates of fibroblasts derived from E13.5 *Fzd7*$^{+/+}$ and *Fzd7*$^{hF7/hF7}$ mice. F7-Ab reacts with the Fzd7$^{P188L}$ protein from *Fzd7*$^{hF7/hF7}$ mice but not with wild-type Fzd7 protein. **D,** F7L6 specifically activates Fzd7$^{P188L}$ from *Fzd7*$^{hF7/hF7}$ MEFs carrying Wnt reporter, 7TGC. Top, representative flow plots. Bottom, data represented as mean ± SEM from three independent experiments. For statistical analyses: one-way ANOVA and Dunnett multiple comparisons test: ***, $P \le 0.001$; **, $P \le 0.01$; *, $P \le 0.05$.

datasets, we found elevated median *FZD7* expression in BRCA, GBM, LUSC, OV, prostate adenocarcinoma (PRAD), and uterine carcinosarcoma (UCS) studies. Upon closer inspection of TCGA BRCA and OV samples, we identified higher *FZD7* expression in triple-negative breast cancer and mesenchymal and proliferative ovarian cancer subtypes, all of which correlate with poorer overall survival. In addition, we observed high FZD7 protein expression in ovarian carcinomas and low FZD7 in normal ovary tissues by IHC, indicating

**Table 1.** Summary of septuximab vedotin toxicity study in *Fzd7*$^{hF7/hF7}$ mice.

| | | | | Histopathologic changes | | | | | | | | |
|---|---|---|---|---|---|---|---|---|---|---|---|---|
| **Genotype** | **Sex** | **Tx** | **% Weight change** | **Brain** | **Eye** | **Heart** | **Kidney** | **Liver** | **Ovary or testis** | **Skin** | **Small intestine** | **Spleen** |
| *Fzd7*$^{hF7/hF7}$ | F | None | −1.4% | – | – | – | – | – | – | – | – | – |
| | | ADC | −1.4% | None | None | None | None | None | None | None | None | None |
| | | | −1.5% | None | None | None | None | None | None | None | None | None |
| | M | None | +3.1% | – | – | – | – | – | – | – | – | – |
| | | ADC | −10.8% | None | None | None | None | None | None | None | None | None |
| | | | +13.2% | None | None | None | None | None | None | None | None | None |
| *Fzd7*$^{+/+}$ | F | None | −3.2% | – | – | – | – | – | – | – | – | – |
| | | ADC | −3.7% | None | None | None | None | None | None | None | None | None |
| | | | −4.4% | None | None | None | None | None | None | None | None | None |
| | M | None | −0.8% | – | – | – | – | – | – | – | – | – |
| | | ADC | −2.3% | None | None | None | None | None | None | None | None | None |
| | | | −1.9% | None | None | None | None | None | None | None | None | None |

Note: *Fzd7*$^{hF7/hF7}$ and *Fzd7*$^{+/+}$ mice were untreated or given a single intravenous dose of F7-ADC (10 mg/kg). Mice were weighed prior to injection (day 0) and seven days after (day 7). H&E staining was performed on the indicated organs harvested on day 7. The study was blinded for histopathologic analyses and no tissue damage was detected.

that FZD7 could serve as a tumor-specific antigen. By mining TCGA data and performing histologic analyses, we validated that FZD7 is a viable candidate for targeted cancer therapies against the WNT pathway.

F7-ADC is a chimeric human–mouse IgG1 antibody conjugated by MC-VC-PABC linkers to four MMAE molecules, on average. We confirmed that F7-ADC selectively binds FZD7 on human cancer cells, then internalized to the lysosomes of target cells, where cathepsin B cleaves the linkers and releases the payload drug, MMAE. F7-ADC treatment of FZD7-high ovarian cancer cells, such as MA-148 and PA-1, induced direct cytotoxicity *in vitro* and tumor xenograft regression in nude mouse models. Furthermore, high-dose F7-ADC treatment did not result in toxicities at the organism or tissue level in *Fzd7*$^{hF7/hF7}$ mice, which we engineered to express Fzd7 receptors carrying the P188L mutation necessary for F7-ADC binding. The lack of toxicity even in tissues known to express Fzd7, such as the small intestine (51), is possibly due to low expression levels, because tumor cell lines with low FZD7 levels (e.g., OVCAR-3) tolerated high F7-ADC concentrations *in vitro*. In future studies, it will be worth exploring the anti-tumor activity of F7-ADC in immunocompetent mouse models, such as the MMTV-Wnt1 mouse tumor model where Fzd7 expression is upregulated (34). In this setting, F7-ADC may engage host innate and adaptive immunity to potentiate tumor regression through mechanisms, such as antibody-dependent cellular cytotoxicity (ADCC) or antibody-dependent cellular phagocytosis (ADCP). Because F7-ADC does not recognize mouse Fzd7, developing a syngeneic mouse model would require engineering the Fzd7$^{P188L}$ mutation in mouse tumor cells or crossing our *Fzd7*$^{hF7/hF7}$ mice with an existing genetically engineered mouse tumor model. Generating such *in vivo* models would provide valuable insight into F7-ADC efficacy and potential adverse effects in an immunocompetent system.

Of note, in contrast to vantictumab, we did not observe inhibitory effects of our unmodified FZD7 antibody on cancer cell growth. This lack of effect may be attributed to the fact that our antibody engages FZD7 in the linker region between the cysteine rich domain (CRD) and the first transmembrane domain. Although FZD7-antibody (F7-Ab) complexes are effectively internalized, an essential feature for antibody and antibody-drug conjugate efficacy, F7-Ab does not block WNT binding to the CRD. In a previous study, we showed that an antigen binding fragment (Fab) of F7-Ab reduced Wnt3a signaling in human embryonic stem cells only when cells were pre-incubated with the Fab (47). Simultaneous addition of Wnt3a and Fab had no detectable effect on Wnt signal transduction, indicating that Fab binding to the linker region did not interfere with Wnt3a signaling. Vantictumab, on the other hand, binds the CRD and effectively blocks WNT binding and signaling (11). Additionally, vantictumab's tumor inhibitory effects may be attributable to its ability to bind multiple FZD receptors (FZD1, 2, 5, 7 and 8) that singly or collectively may play crucial roles in cell proliferation.

In recent years, ADCs have emerged as a powerful modality to target a variety of cancers, with an increasing number of ADCs receiving approval for oncotherapies (reviewed in (53, 54)). This current study highlights the potential for septuximab vedotin as a novel treatment of ovarian cancer. Current treatment options for ovarian cancer are limited, and standard of care involves aggressive surgical efforts to debulk the cancer and neoadjuvant chemotherapy. Critical to the development of this ADC will be the identification of suitable biomarkers for the early detection of ovarian cancer.

Our preclinical F7-ADC data demonstrates therapeutic efficacy and exquisite specificity to FZD7 *in vitro* and *in vivo* with no toxicity in the *Fzd7*$^{hF7/hF7}$ mouse model. By targeted killing of FZD7-positive cancer cells, rather than globally inhibiting WNT signaling, we predict that the bone-related adverse events frequently associated with WNT-targeting drugs will be mitigated. Moreover, FZD7 expression has been implicated in multiple cancers with poor patient prognoses. In ovarian cancer, FZD7 expression correlated with resistance to platinum-based chemotherapy, tumor initiation, and cancer stem cell proliferation (55, 56). In additional examples, FZD7 was associated with epithelial-mesenchymal transition in triple-negative breast cancer (57), cisplatin and paclitaxel resistance in uterine cancer (58), and tumor proliferation in gastric cancer (26). As such, the F7-ADC approach may provide a powerful biomarker-driven therapy to combat a variety of aggressive solid tumors overexpressing FZD7.

## Authors' Disclosures

C. Patel reports personal fees from Roche outside the submitted work. J.P. Mesirov reports grants from NIH/NCI during the conduct of the study. D.A. Carson reports a patent for US 10,766,962 B2; issued September 8, 2020 issued. S.J. Advani reports grants from NIH during the conduct of the study. K. Willert reports grants from NIH/NIGMS and grants from The Mary Kay Foundation during the conduct of the study; in addition, K. Willert has a patent for US 10766962-B2 issued. No disclosures were reported by the other authors.

## Disclaimer

The content is solely the responsibility of the authors and does not necessarily represent the official views of the NIH. The authors declare no competing financial interests.

## Authors' Contributions

**M. Do:** Conceptualization, data curation, formal analysis, investigation, methodology, writing–original draft. **C.C.N. Wu:** Data curation, investigation, methodology. **P.R. Sonavane:** Investigation, methodology. **E.F. Juarez:** Data curation, software. **S.R. Adams:** Resources, methodology. **J. Ross:** Investigation, methodology. **A. Rodriguez y Baena:** Investigation. **C. Patel:** Data curation, formal analysis. **J.P. Mesirov:** Software, formal analysis, funding acquisition. **D.A. Carson:** Conceptualization, supervision, funding acquisition, writing–review and editing. **S.J. Advani:** Resources, funding acquisition, methodology, writing–review and editing. **K. Willert:** Conceptualization, resources, supervision, funding acquisition, investigation, project administration, writing–review and editing.

## Acknowledgments

We are grateful to UCSD Transgenic Mouse Services for technical assistance with generating *Fzd7*$^{hF7/hF7}$ mice; UCSD Tissue Technology Shared Resource for performing H&E and IHC staining; Dr. Nissi Varki (UCSD) for IHC analyses; Jesus Olvera and Cody Fine (UCSD) for technical assistance with flow cytometry experiments; UCSD Nikon Imaging Center for technical assistance with confocal imaging; and Dr. Dina Hingorani and Maria Fernanda Camargo (UCSD) for initial help with F7-ADC synthesis and tumor xenograft mouse models. Research reported in this publication was supported by grants from the NIH (NIGMS, R35GM134961) and The Mary Kay Foundation Cancer Research Grant Program (to K. Willert); NIH (NCI, R37CA215081; to S.J. Advani); NIH (NCI, U24CA248457; to J.P. Mesirov). M. Do was supported in part by a Cancer Biology, Informatics, Omics Training Program from the NCI (T32CA067754). The UCSD Tissue Technology Shared Resource is supported by a NCI Cancer Center Support Grant (CCSG grant P30CA23100).

The costs of publication of this article were defrayed in part by the payment of page charges. This article must therefore be hereby marked *advertisement* in accordance with 18 U.S.C. Section 1734 solely to indicate this fact.

Received June 20, 2021; revised August 27, 2021; accepted October 11, 2021; published first October 19, 2021.

## References

1. Niehrs C. The complex world of WNT receptor signalling. Nat Rev Mol Cell Biol 2012;13:767–79.
2. Groden J, Thliveris A, Samowitz W, Carlson M, Gelbert L, Albertsen H, et al. Identification and characterization of the familial adenomatous polyposis coli gene. Cell 1991;66:589–600.
3. Mazzoni SM, Fearon ER. AXIN1 and AXIN2 variants in gastrointestinal cancers. Cancer Lett 2014;355:1–8.
4. Clevers H, Loh KM, Nusse R. Stem cell signaling. An integral program for tissue renewal and regeneration: Wnt signaling and stem cell control. Science 2014;346:1248012.
5. Kim S, Jeong S. Mutation hotspots in the beta-catenin gene: lessons from the human cancer genome databases. Mol Cells 2019;42:8–16.
6. Seshagiri S, Stawiski EW, Durinck S, Modrusan Z, Storm EE, Conboy CB, et al. Recurrent R-spondin fusions in colon cancer. Nature 2012;488:660–4.
7. Spit M, Fenderico N, Jordens I, Radaszkiewicz T, Lindeboom RG, Bugter JM, et al. RNF43 truncations trap CK1 to drive niche-independent self-renewal in cancer. EMBO J 2020;39:e103932.
8. Zeng CM, Chen Z, Fu L. Frizzled receptors as potential therapeutic targets in human cancers. Int J Mol Sci 2018;19:1543.
9. Jung YS, Park JI. Wnt signaling in cancer: therapeutic targeting of Wnt signaling beyond beta-catenin and the destruction complex. Exp Mol Med 2020;52:183–91.
10. Davis SL, Cardin DB, Shahda S, Lenz HJ, Dotan E, O'Neil BH, et al. A phase 1b dose escalation study of Wnt pathway inhibitor vantictumab in combination with nab-paclitaxel and gemcitabine in patients with previously untreated metastatic pancreatic cancer. Invest New Drugs 2020;38:821–30.
11. Gurney A, Axelrod F, Bond CJ, Cain J, Chartier C, Donigan L, et al. Wnt pathway inhibition via the targeting of Frizzled receptors results in decreased growth and tumorigenicity of human tumors. Proc Natl Acad Sci U S A 2012;109:11717–22.
12. Mita MM, Becerra C, Richards DA, Mita AC, Shagisultanova E, Osborne CRC, et al. Phase 1b study of WNT inhibitor vantictumab (VAN, human monoclonal antibody) with paclitaxel (P) in patients (pts) with 1st- to 3rd-line metastatic HER2-negative breast cancer (BC). J Clin Oncol 2016;34:2516.
13. Smith DC, Rosen LS, Chugh R, Goldman JW, Xu L, Kapoun A, et al. First-in-human evaluation of the human monoclonal antibody vantictumab (OMP-18R5; anti-Frizzled) targeting the WNT pathway in a phase I study for patients with advanced solid tumors. J Clin Oncol 2013;31:2540.
14. Giraudet AL, Cassier PA, Iwao-Fukukawa C, Garin G, Badel JN, Kryza D, et al. A first-in-human study investigating biodistribution, safety and recommended dose of a new radiolabeled MAb targeting FZD10 in metastatic synovial sarcoma patients. BMC Cancer 2018;18:646.
15. Vaisitti T, Arruga F, Vitale N, Lee TT, Ko M, Chadburn A, et al. ROR1 targeting with the antibody-drug conjugate VLS-101 is effective in Richter syndrome patient-derived xenograft mouse models. Blood 2021;137:3365–77.
16. Damelin M, Bankovich A, Bernstein J, Lucas J, Chen L, Williams S, et al. A PTK7-targeted antibody-drug conjugate reduces tumor-initiating cells and induces sustained tumor regressions. Sci Transl Med 2017;9:eaag2611.
17. Fischer MM, Cancilla B, Yeung VP, Cattaruzza F, Chartier C, Murriel CL, et al. WNT antagonists exhibit unique combinatorial antitumor activity with taxanes by potentiating mitotic cell death. Sci Adv 2017;3:e1700090.
18. Jimeno A, Gordon M, Chugh R, Messersmith W, Mendelson D, Dupont J, et al. A first-in-human phase I study of the anticancer stem cell agent ipafricept (OMP-54F28), a decoy receptor for Wnt ligands, in patients with advanced solid tumors. Clin Cancer Res 2017;23:7490–7.
19. Moore KN, Gunderson CC, Sabbatini P, McMeekin DS, Mantia-Smaldone G, Burger RA, et al. A phase 1b dose escalation study of ipafricept (OMP54F28) in combination with paclitaxel and carboplatin in patients with recurrent platinum-sensitive ovarian cancer. Gynecol Oncol 2019;154:294–301.
20. Madan B, Ke Z, Harmston N, Ho SY, Frois AO, Alam J, et al. Wnt addiction of genetically defined cancers reversed by PORCN inhibition. Oncogene 2016;35:2197–207.
21. Day TF, Guo X, Garrett-Beal L, Yang Y. Wnt/beta-catenin signaling in mesenchymal progenitors controls osteoblast and chondrocyte differentiation during vertebrate skeletogenesis. Dev Cell 2005;8:739–50.
22. Maeda K, Kobayashi Y, Udagawa N, Uehara S, Ishihara A, Mizoguchi T, et al. Wnt5a-Ror2 signaling between osteoblast-lineage cells and osteoclast precursors enhances osteoclastogenesis. Nat Med 2012;18:405–12.
23. Ng M, Tan DS, Subbiah V, Weekes CD, Teneggi V, Diermayr V, et al. First-in-human phase 1 study of ETC-159 an oral PORCN inhbitor in patients with advanced solid tumours. J Clin Oncol 2017;35:2584.
24. Tan D, Ng M, Subbiah V, Messersmith W, Teneggi V, Diermayr V, et al. 71O - Phase I extension study of ETC-159 an oral PORCN inhibitor administered with bone protective treatment, in patients with advanced solid tumours. Ann Oncol 2018;29:ix23–ix4.
25. Madan B, McDonald MJ, Foxa GE, Diegel CR, Williams BO, Virshup DM. Bone loss from Wnt inhibition mitigated by concurrent alendronate therapy. Bone Res 2018;6:17.
26. Flanagan DJ, Barker N, Costanzo NSD, Mason EA, Gurney A, Meniel VS, et al. Frizzled-7 is required for Wnt signaling in gastric tumors with and without Apc mutations. Cancer Res 2019;79:970–81.

27. Kirikoshi H, Sekihara H, Katoh M. Up-regulation of Frizzled-7 (FZD7) in human gastric cancer. Int J Oncol 2001;19:111–5.
28. Ueno K, Hazama S, Mitomori S, Nishioka M, Suehiro Y, Hirata H, et al. Down-regulation of frizzled-7 expression decreases survival, invasion and metastatic capabilities of colon cancer cells. Br J Cancer 2009;101:1374–81.
29. Vincan E, Darcy PK, Smyth MJ, Thompson EW, Thomas RJ, Phillips WA, et al. Frizzled-7 receptor ectodomain expression in a colon cancer cell line induces morphological change and attenuates tumor growth. Differentiation 2005;73: 142–53.
30. Merle P, de la Monte S, Kim M, Herrmann M, Tanaka S, Von Dem Bussche A, et al. Functional consequences of frizzled-7 receptor overexpression in human hepatocellular carcinoma. Gastroenterology 2004;127:1110–22.
31. Merle P, Kim M, Herrmann M, Gupte A, Lefrancois L, Califano S, et al. Oncogenic role of the frizzled-7/beta-catenin pathway in hepatocellular carcinoma. J Hepatol 2005;43:854–62.
32. Asad M, Wong MK, Tan TZ, Choolani M, Low J, Mori S, et al. FZD7 drives in vitro aggressiveness in Stem-A subtype of ovarian cancer via regulation of non-canonical Wnt/PCP pathway. Cell Death Dis 2014;5:e1346.
33. Tan M, Asad M, Heong V, Wong MK, Tan TZ, Ye J, et al. The FZD7-TWIST1 axis is responsible for anoikis resistance and tumorigenesis in ovarian carcinoma. Mol Oncol 2019;13:757–80.
34. Chakrabarti R, Wei Y, Hwang J, Hang X, Andres Blanco M, Choudhury A, et al. DeltaNp63 promotes stem cell activity in mammary gland development and basal-like breast cancer by enhancing Fzd7 expression and Wnt signalling. Nat Cell Biol 2014;16:1004–15, 1–13.
35. Xie W, Zhao H, Wang F, Wang Y, He Y, Wang T, et al. A novel humanized Frizzled-7-targeting antibody enhances antitumor effects of Bevacizumab against triple-negative breast cancer via blocking Wnt/beta-catenin signaling pathway. J Exp Clin Cancer Res 2021;40:30.
36. Yang L, Wu X, Wang Y, Zhang K, Wu J, Yuan YC, et al. FZD7 has a critical role in cell proliferation in triple negative breast cancer. Oncogene 2011;30: 4437–46.
37. Deng B, Zhang S, Miao Y, Zhang Y, Wen F, Guo K. Down-regulation of Frizzled-7 expression inhibits migration, invasion, and epithelial-mesenchymal transition of cervical cancer cell lines. Med Oncol 2015;32:102.
38. Tiwary S, Xu L. FRIZZLED7 is required for tumor initiation and metastatic growth of melanoma cells. PLoS One 2016;11:e0147638.
39. King TD, Zhang W, Suto MJ, Li Y. Frizzled7 as an emerging target for cancer therapy. Cell Signal 2012;24:846–51.
40. Phesse T, Flanagan D, Vincan E. Frizzled7: a promising Achilles' heel for targeting the Wnt receptor complex to treat cancer. Cancers 2016;8:50.
41. Adams SR, Yang HC, Savariar EN, Aguilera J, Crisp JL, Jones KA, et al. Anti-tubulin drugs conjugated to anti-ErbB antibodies selectively radiosensitize. Nat Commun 2016;7:13019.
42. Hingorani DV, Doan MK, Camargo MF, Aguilera J, Song SM, Pizzo D, et al. Precision chemoradiotherapy for HER2 tumors using antibody conjugates of an auristatin derivative with reduced cell permeability. Mol Cancer Ther 2020;19: 157–67.
43. Gumber D, Do M, Suresh Kumar N, Sonavane PR, Wu CCN, Cruz LS, et al. Selective activation of FZD7 promotes mesendodermal differentiation of human pluripotent stem cells. Elife 2020;9:e63060.
44. Rahman M, Jackson LK, Johnson WE, Li DY, Bild AH, Piccolo SR. Alternative preprocessing of RNA-Sequencing data in The Cancer Genome Atlas leads to improved analysis results. Bioinformatics 2015;31:3666–72.
45. Verhaak RG, Tamayo P, Yang JY, Hubbard D, Zhang H, Creighton CJ, et al. Prognostically relevant gene signatures of high-grade serous ovarian carcinoma. J Clin Invest 2013;123:517–25.
46. Aysola K, Desai A, Welch C, Xu J, Qin Y, Reddy V, et al. Triple negative breast cancer - an overview. Hereditary Genet 2013;2013:001.
47. Fernandez A, Huggins IJ, Perna L, Brafman D, Lu D, Yao S, et al. The WNT receptor FZD7 is required for maintenance of the pluripotent state in human embryonic stem cells. Proc Natl Acad Sci U S A 2014;111:1409–14.
48. Jain N, Smith SW, Ghone S, Tomczuk B. Current ADC linker chemistry. Pharm Res 2015;32:3526–40.
49. Yu H, Ye X, Guo N, Nathans J. Frizzled 2 and frizzled 7 function redundantly in convergent extension and closure of the ventricular septum and palate: evidence for a network of interacting genes. Development 2012; 139:4383–94.
50. Fuerer C, Nusse R. Lentiviral vectors to probe and manipulate the Wnt signaling pathway. PLoS One 2010;5:e9370.
51. Flanagan DJ, Phesse TJ, Barker N, Schwab RH, Amin N, Malaterre J, et al. Frizzled7 functions as a Wnt receptor in intestinal epithelial Lgr5(+) stem cells. Stem Cell Reports 2015;4:759–67.
52. Sato T, van Es JH, Snippert HJ, Stange DE, Vries RG, van den Born M, et al. Paneth cells constitute the niche for Lgr5 stem cells in intestinal crypts. Nature 2011;469:415–8.
53. Baah S, Laws M, Rahman KM. Antibody-drug conjugates-a tutorial review. Molecules 2021;26:2943.
54. Jin Y, Schladetsch MA, Huang X, Balunas MJ, Wiemer AJ. Stepping forward in antibody-drug conjugate development. Pharmacol Ther 2021:107917.
55. Condello S, Sima L, Ivan C, Cardenas H, Schiltz G, Mishra RK, et al. Tissue tranglutaminase regulates interactions between ovarian cancer stem cells and the tumor niche. Cancer Res 2018;78:2990–3001.
56. Wang Y, Zhao G, Condello S, Huang H, Cardenas H, Tanner EJ, et al. Frizzled-7 identifies platinum-tolerant ovarian cancer cells susceptible to ferroptosis. Cancer Res 2021;81:384–99.
57. Yin P, Bai Y, Wang Z, Sun Y, Gao J, Na L, et al. Non-canonical Fzd7 signaling contributes to breast cancer mesenchymal-like stemness involving Col6a1. Cell Commun Signal 2020;18:143.
58. Choijamts B, Jimi S, Kondo T, Naganuma Y, Matsumoto T, Kuroki M, et al. CD133+ cancer stem cell-like cells derived from uterine carcinosarcoma (malignant mixed Mullerian tumor). Stem Cells 2011;29:1485–95.